JMEPEG (2012) 21:247–252
DOI: 10.1007/s11665-011-9867-6

1059-9495/$19.00

Mechanical Properties of Squeeze-Cast A356 Composites Reinforced With B_4C Particulates

Ali Mazahery and Mohsen Ostad Shabani

(Submitted September 25, 2010; in revised form January 22, 2011)

In this study, different volume fractions of B_4C particles were incorporated into the aluminum alloy by a mechanical stirrer, and squeeze-cast A356 matrix composites reinforced with B_4C particles were fabricated. Microstructural characterization revealed that the B_4C particles were distributed among the dendrite branches, leaving the dendrite branches as particle-free regions in the material. It also showed that the grain size of aluminum composite is smaller than that of monolithic aluminum. X-ray diffraction studies also confirmed the existence of boron carbide and some other reaction products such as AlB_2 and Al_3BC in the composite samples. It was observed that the amount of porosity increases with increasing volume fraction of composites. The porosity level increased, since the contact surface area was increased. Tensile behavior and the hardness values of the unreinforced alloy and composites were evaluated. The strain-hardening behavior and elongation to fracture of the composite materials appeared very different from those of the unreinforced Al alloy. It was noted that the elastic constant, strain-hardening and the ultimate tensile strength (UTS) of the MMCs are higher than those of the unreinforced Al alloy and increase with increasing B_4C content. The elongation to fracture of the composite materials was found very low, and no necking phenomenon was observed before fracture. The tensile fracture surface of the composite samples was indicative of particle cracking, interface debonding, and deformation constraint in the matrix and revealed the brittle mode of fracture.

Keywords aluminum, boron carbide, metal matrix composites, stir casting

1. Introduction

Metal matrix composites (MMCs) are attractive materials to be employed in various applications because of their improved properties. A vast range of MMC materials has been conceived and studied to combine the desirable attributes of metal and ceramics. The addition of high strength, high modulus refractory particles to a ductile metal matrix produces a material whose mechanical properties are intermediate between the matrix alloy and ceramic reinforcement. Metals have a useful combination of properties such as high strength, ductility, and high temperature resistance but sometimes have low stiffness, whereas ceramics are stiff and strong though brittle. In addition to improved physical and mechanical properties, particulate-reinforced composites are generally isotropic, and they can be processed through conventional methods used for metals (Ref 1, 2).

Matrices based on Ag, Al, Be, Co, Cu, Fe, Mg, Ni, and Ti are all commercially produced and used. By far, the largest commercial volumes are for aluminum matrix composites (AMCs), which accounts for 69% by mass of the annual MMC production (Ref 3). This large commercial volume is the result of their excellent physical, mechanical, and tribological properties and also because of good combination of thermal conductivity and dimensional stability properties (Ref 4-8).

The conventional reinforcement materials for AMCs are SiC and Al_2O_3. Owing to the higher cost of B_4C powder relative to SiC and Al_2O_3, research has been conducted on a limited basis on B_4C reinforced MMCs (Ref 9). Monolithic B_4C ceramic is a low-density material that is very hard, strong, and stiff. However, densification of monolithic B_4C requires high temperatures and/or application of high pressures (Ref 10).

A356-B_4C composites have the potential to combine the high stiffness and hardness of B_4C with the ductility of Al and result in a strong low-density material. These boron carbides (B_4Cs) react strongly with Al, resulting in a variety of binary and ternary compounds, including Al_3BC, $AlB_{24}C_4$ (commonly designated as AlB_{10}), $Al_8B_4C_7$, $Al_3B_{48}C_2$ (often known as β-AlB_{12}), AlB_2, $AlB_{12}C_2$, $AlB_{48}C_2$, Al_4C_3, and α-AlB_{12} (Ref 11).

According to the type of reinforcement, the fabrication techniques can vary considerably. These techniques include squeeze casting, liquid metal infiltration, spray decomposition, and powder metallurgy. The squeeze casting offers good micro structural control at relatively low cost. The pressure applied during solidification in the squeeze-casting technique results in excellent feeding during solidification shrinkage (Ref 12, 13).

Composite mechanical property enhancement is a function of the volume fraction, size, shape, and spatial distribution of the reinforcement, and is also dependent on how well the externally applied load is transferred to the reinforcing phase. Stronger adhesion at the particle/matrix interface improves load transfer, increasing the yield strength and stiffness, and delays the onsets of particle/matrix de-cohesion (Ref 14).

Ali Mazahery, School of Metallurgy and Materials Engineering, University of Tehran, Tehran, Iran; and **Mohsen Ostad Shabani**, Materials and Energy Research Center (MERC), P.O. Box 14155-4777, Tehran, Iran. Contact e-mails: vahid_ostadshabany@yahoo.com and ostadshabany@yahoo.com.

In this study, the A356-B_4C composites have been processed using squeeze casting. B_4C powder was chosen as reinforcement material because of its higher hardness (2900-3580 kg/mm^2) than the conventional and routinely used reinforcement materials such as SiC, Al_2O_3, etc. Further, its density (2.52 g/cm^3) is very close to that of Al alloy matrix. The results of the mechanical properties of squeeze-cast composites are presented in this article.

2. Experimental Procedure

In this study, a commercial casting-grade aluminum alloy (A356) {(wt.%): 7.5 Si, 0.38 Mg, 0.02 Zn, 0.001 Cu, 0.106 Fe, and Al (balance)} was employed as the matrix material, while the B_4C particles with particle size ranging from 1 to 5 μm were used as the reinforcements. The grain size of B_4C particles was analyzed using a Malvern laser size analyzer.

For manufacturing of the MMCs, 5, 7.5, 10, 12.5, and 15 vol.% B_4C particles were used. The melt-particle slurry has been produced by mechanical stirrer. Approximately, 450 g of A356 alloy was charged into the graphite crucible and heated up to a temperature above the alloy's melting point (750 °C). The temperature control of the electric furnace and molten metal is carried out using an NR911 type thermostat. This thermostat has a special control unit and thermocouples. Thermocouples were inserted into the melt and the furnace to measure their temperatures. The graphite stirrer fixed on the mandrel of the drilling machine was introduced into the melt and positioned just below the surface of the melt. Approximately, 1 g reinforcement and aluminum powder mixture were inserted into an aluminum foil by forming a packet. The packets were added into molten metal of crucible when the vortex was formed at every 20 s. The packet of mixture melted, and the particles started to distribute around the alloy sample. It was stirred at a speed of approximately 600 rpm. Argon gas was also blown into the crucible during the operation. The squeeze casting was obtained by pouring the composite slurry into preheated permanent die and punch. It is then allowed to solidify under a squeeze pressure of 80 MPa for a duration of 5 min. High temperature graphite powder was used in the die to facilitate the removal of cast blanks from the die after cooling.

The as-cast samples were all treated according to T6 condition: solution treated at 540 °C for 8 h followed by water-quenching and 155 °C artificial aging for 16 h.

For microstructure study, specimens were prepared by grinding through 120, 400, 600, and 800 grit papers followed by polishing with 6-μm diamond paste and etched with Keller's reagent (2 mL HF (48%), 3 mL HCl (conc.), 5 mL HNO_3 (conc.), and 190 mL water). Microscopic examinations of the composites and matrix alloy were carried out using an optical microscope. X-ray diffraction (DebyeScherrer) and energy dispersive x-ray analyses (EDXA) were performed to determine the chemical compositions of the matrix and the reinforcement.

The experimental density of the composites was obtained by the Archimedian method of weighing small pieces cut from the composite cylinder first in air and then in water, while the theoretical density was calculated using the mixture rule according to the weight fraction of the B_4C particles. The porosities of the produced composites were evaluated from the difference between the expected and the observed density of each sample. To study the hardness, the Brinell hardness values of the samples were measured on the polished samples using an indenter ball with 2.5-mm diameter at a load of 31.25 kg. For each sample, five hardness readings on randomly selected regions were taken to eliminate possible segregation effects and get a representative value of the matrix material hardness. During hardness measurement, precaution was taken to make indentation at a distance of at least twice the diagonal length of the previous indention.

The tensile tests were used to assess the mechanical behaviors of the composites and matrix alloy. The composite and matrix alloy rods were machined to tensile specimens according to ASTM.B 557 standard. The load-displacement diagram and the load-displacement data were recorded from the digital display attached with the equipment. These load and displacement data were transformed to true stress and true strain data using the standard methodology, and ultimate tensile strength (UTS) values were obtained. Each value of UTS is an average of at least three tensile specimens. Fractography was done on the fractured surface using a scanning electron microscope (SEM).

3. Results and Discussion

Figure 1 shows optical micrograph of the MMC. Because of the casting process, the B_4C particles were distributed between the dendrite branches and were frequently clustered together, leaving the dendrite branches as particle-free regions in the material. The distribution of the B_4C particles was fairly uniform under low magnification, but obviously not uniform microscopically. In order to determine the composition of the present phases, energy dispersion spectrum (EDS analysis) is

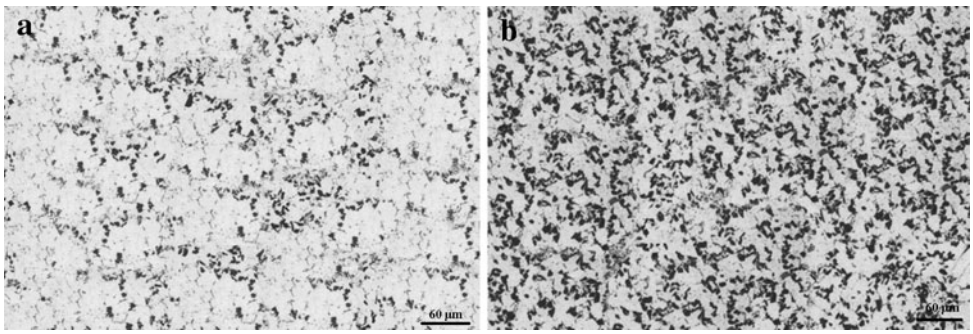

Fig. 1 Typical optical micrographs: (a) the composite with 5 vol.% B4C, (b) the composite with 15 vol.% B4C

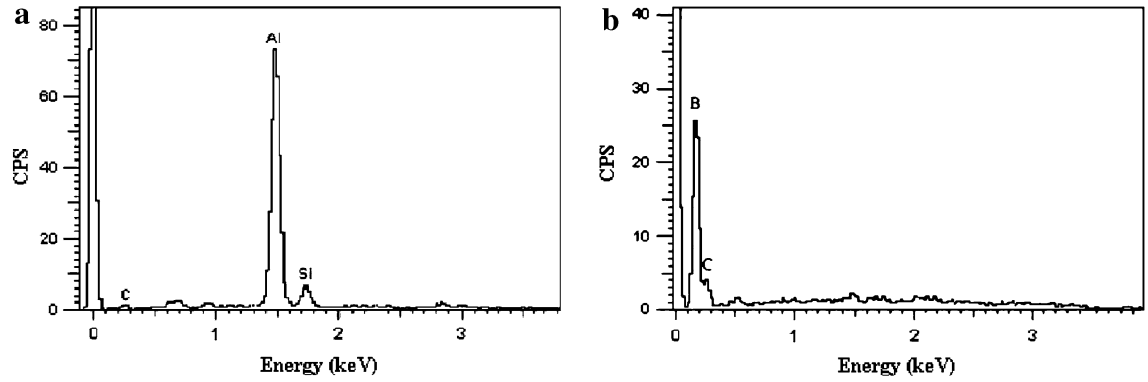

Fig. 2 EDX spectrum of (a) Al alloy, and (b) B4C particles

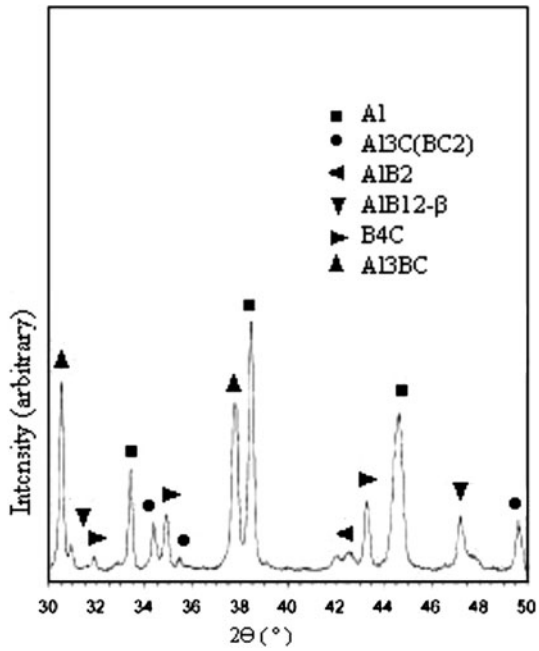

Fig. 3 XRD pattern of the composite produced with 10 vol.% B4C at 750 °C

implemented on Al matrix and B_4C particles, and the results are depicted in Fig. 2. According to the compositional information, it is evident that B and C peaks correspond to composition of B_4C particles.

Figure 3 shows the XRD pattern of the composite produced with 10 vol.% B_4C at 750 °C. It can be seen that B_4C and aluminum are present in the sample. The results for other samples were also similar to this one. In general, the XRD results showed that A356-B_4C composites produced under the present processing conditions are composed of various combinations of Al_3BC, AlB_2, and AlB_{12} phases. The types of these phases and their quantities depend on processing conditions. Dissolution of the carbide rapidly saturates the melt with boron and carbon since the maximum solubility of these two elements in aluminum is relatively low (0.1 wt.% and a few tenths of a ppm). Subsequently, AlB_2 nucleates on impurity seeds from the supersaturated melt, while the Al_3BC phase nucleates at the B_4C surface. Growth continues via a classical dissolution-precipitation mechanism (Ref 15).

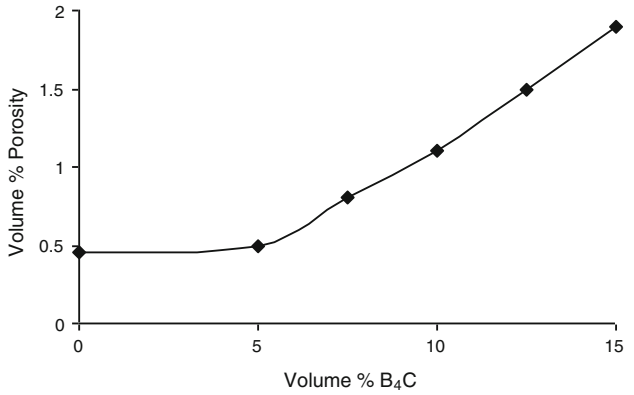

Fig. 4 Variations of porosity of the squeeze-cast composites as a function of B4C content

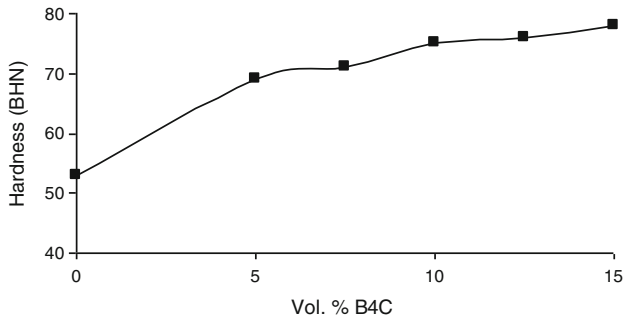

Fig. 5 Variations of hardness value of the samples as a function of B4C content

Figure 4(a) shows the variation of porosity with the B_4C content. It indicates that increasing amount of porosity is observed with increasing the volume fraction of composites. The porosity level increased, since the contact surface area was increased. It has also been reported by the earlier studies (Ref 16, 17). The increased porosity level is attributed to the increasing surface gas layers surrounding particles, increasing effective viscosity of suspension resulting in a higher gas hold up as well as improper filling of the gaps between adjacent particles, and increasing sites for heterogeneous pore nucleation (Ref 18-20).

The results of hardness tests are shown in Fig. 5. For composite materials containing a soft matrix and a hard

reinforcing phase, as in the case of particle-reinforced composites, the selection of the region in the sample for evaluating the hardness data is very crucial. In order to obtain the average values of hardness, predominant areas in the soft matrix or the hard reinforcing phase should be avoided, so that the average values of hardness are attained from these measurements. The hardness of the MMCs increases with the volume fraction of particulates in the alloy matrix. The higher hardness of the composites could be because B_4C particles act as obstacles to the motion of dislocation (Ref 21-25). As shown, hardness increases with the amount of the B_4C particles present. The dispersion of B_4C particles enhances the hardness: as these particles are harder than Al alloy, the materials render their inherent property of hardness to the soft matrix.

Figure 6 shows the typical stress-strain curves obtained from uniaxial tension tests. The curves in this figure are for unreinforced AI alloy (A) and MMC materials containing 5 (B), 10 (C), and 15 (D) vol.% B_4C. It is apparent that the slope of the linear portion of the MMC curves is greater than that of the unreinforced Al alloy. Obviously, the increase of the elastic constant of composite was caused by the addition of the B_4C particles. The considerable increase of strain-hardening observed during plastic deformation is also rationalized, attributing it to the resistance of the hard reinforcing particles to slip behavior of the Al matrix. The elongation to fracture of the composite materials was found very low, and no necking phenomenon was observed before fracture. On the other hand, the elongation to fracture of the unreinforced Al alloy was about 15 percentages.

In the case of composites, the plastic flow of matrix is constrained because of the presence of these rigid and very strong B_4C particles. It has been understood that the plastic flow of the composite is due to the plastic flow of the matrix. The strain-hardening of the composite is primarily due to hardening of the matrix during its plastic flow. The strain-hardening of matrix is expected to be influenced by the following factors: (i) dislocation density and dislocation-to-dislocation interaction, and (ii) constraint of plastic flow due to resistance offered by B_4C-particles. The dislocation density in the matrix of the composite might be increased with increase in B_4C (Ref 26). To keep the continuity of the composite material under the external load, which requires no formation of any voids and cracks along the particle-matrix

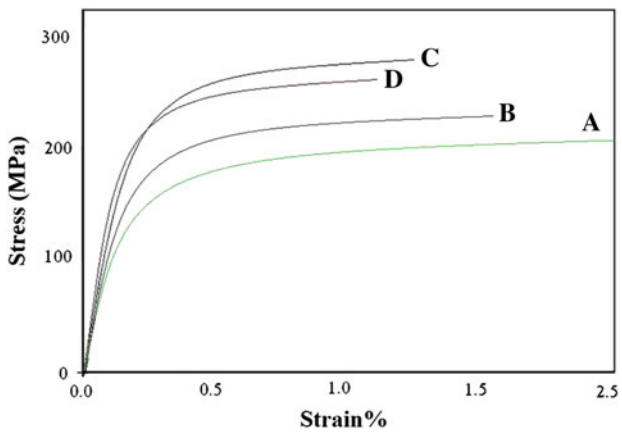

Fig. 6 Stress-strain curves for unreinforced Al alloy failing at 15% (A), Al/5 vol.% B4C failing at 1.7% (B), Al/10 vol.% B4C (C), and Al/15 vol.% B4C (D)

interface, a strong internal stress would develop between B_4C particles and the matrix (increased dislocation density). It is expected that due to the thermal mismatch stress ($CTE_{B4C} = 5 \times 10^{-6}$), there is a possibility of increased dislocation density within the matrix. The difference between the coefficient of thermal expansion (CTE) values of matrix and ceramic particles generates thermally induced residual stresses and increases dislocations density upon rapid solidification during the fabrication process. This type of internal stress would resist the slip behavior in the metal matrix, and hence, the strain-hardening rate would increase. Similar fact is also true for plastic constraint to the matrix due to particle addition. As seen in Fig. 1, dendrite branches of the Al matrix is surrounded by the B_4C particles, and these particles along the dendrite boundaries act as barriers to the slip behavior of the matrix, thereby strengthening the composite material. This strengthening mechanism is similar to the conventional theory of grain-boundary strengthening in which the grain boundaries block the dislocation movement during plastic deformation. However, this effect of the reinforcing B_4C particles along grain boundaries is obviously much stronger (Ref 27, 28).

The above argument should also hold, at least partially, for rationalizing the contribution of the reinforcing particles to the increase of the elastic constant in discontinuous reinforcement MMCs, since the load-transfer process is also involved in the elastic range (Ref 29, 30).

On the other hand, the microscopic nonuniformity of the particle distribution, created by dendrite structure formation and usually in the form of clustering, is considered as the reason for internal stresses and also stress triaxiality, which are responsible not only for the special hardening behavior, but also for the early appearance of particle cracking, particle interface debonding, and void formation in the matrix. It can also be speculated that the low ductility of the studied MMC is due to the early coalescence of these microdamages (Ref 30, 31).

It can be observed that the composite containing 15 vol.% B_4C exhibits less flow stress than the composite with 10 vol.% in higher strain. As strain increased, more plastic deformation must be accommodated, and the interaction between particle and matrix became more severe, producing even higher internal stress and creating an even stronger state of stress triaxiality. Interface debonding and even particle cracking would then occur in composite with 15 vol.%, since the local superposition of the internal stress and applied stress may become very high. The emergence of all of these behaviors would not only relax the internal stress field around the particles as well as inside the particle clusters, but also decrease the degree of the stress triaxiality which leads to a decrease in strain-hardening rate of composite in higher strain. This might also be the result of greater agglomeration of particles and higher degree of microporosity present in the composite at higher B_4C content. These results are consistent with the trends reported by other investigators (Ref 32).

Figure 7 shows the variations of UTS of the composites with the variations of volume fraction. Note that the volume fraction of ceramic particles quoted in this figure is the sum of all three main present ceramic phases: B_4C, AlB_2, and Al_3BC. Each value of UTS is an average of at least three tensile specimens. The strength of the composites increases with the increase in reinforcement content. According to the results of this experiment, quite significant improvement in strength is noted when 10 vol.% B_4C particles are added; further increase in B_4C content leads to reduction in strength values.

The great enhancement in the values of UTS observed in composites relative to monolithic aluminum is due to grain refinement (Ref 33), the strong multidirectional stress at the A356/B_4C interface, small particle size, and low degree of porosity, which leads to effective transfer of applied tensile load to the uniformly distributed strong B_4C particulates (Ref 29, 30).

The amount of interface area, nevertheless, increases with increase in B_4C content, and the microporosities also increase with increase in B_4C content. On the other hand, increasing dislocation, i.e., defects induced around the B_4C particles due to the differences in the thermal expansion coefficients of Al and B_4C, might result in debonding of the interface and decrease in UTS in the composites with higher B_4C volume fraction (Ref 17). Hereby, it is believed that strengthening and weakening factors of mechanical properties could neutralize the effect of each other and thus, the composite containing 10 vol% B_4C exhibits the maximum ultimate tensile stress.

Results of fracture surface analysis conducted on the tensile fracture samples revealed typical ductile fracture in the case of unreinforced Al alloy (Fig. 8a) with uniform dimples which are mostly deep and circular-shaped, indicating that there was a considerable plastic deformation involved in the void coalescence.

The fracture surface in the case of composite samples (Fig. 8b) revealed the brittle mode of fracture, with clear evidence of particle cracking, interface debonding, and deformation constraint in the matrix (Ref 30). The above microscopic responses in the material during deformation are responsible for the low ductility of the material. Apparently, the existence of the reinforcing B_4C particles has changed the behavior of the fracture process considerably. Two types of dimples can be observed in the Al-reinforced materials: (a) dimples in the particle-free matrix regions and (b) dimples associated with particles. In the particle-free matrix regions, the dimples appeared to be rather similar to those observed in the unreinforced alloy. For the dimples with B_4C particles inside, both the size and shape of the dimples are found to be associated with the B_4C particles. It seems that the matrix-particle interface debonding and particle cracking played the main role in the crack formation. However, it is not clear at what applied strain level, particle cracking occurred and which of the two behaviors, interface debonding or particle cracking, was predominant.

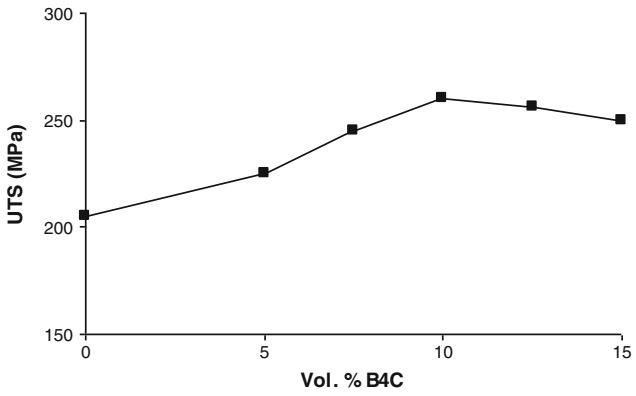

Fig. 7 Variations of UTS value of the samples as a function of vol.% B4C particulates

4. Conclusion

1. In general, B_4C particles are incorporated into aluminum matrix in the A356-B_4C composites produced under the processing conditions of squeeze casting used in this study. The other phases detected by XRD are composed of various combinations of Al_3BC, AlB_2, and AlB_{12}.
2. The B_4C particles were distributed between the dendrite branches and were frequently clustered together, leaving the dendrite branches as particle-free regions in the material.
3. Porosity level increased slightly with increasing particulate content. These results can be attributed to the increased surface area of the B4C particles which can in turn increase the porosity levels.
4. The hardness of the MMCs increases with the volume fraction of particulates in the alloy matrix because of the increasing ceramic phase of the matrix alloy. The higher hardness of the composites could be because B_4C particles act as obstacles to the motion of dislocation.
5. It was noted that the elastic constant, strain-hardening, and UTS of the MMCs is higher than that of the unreinforced Al alloy and increase with increasing B_4C content. The elongation to fracture of the composite materials was found to be very low, and no necking phenomenon was observed before fracture.
6. The tensile fracture surface of the unreinforced Al alloy is clearly indicative of lot of dimples which are mostly

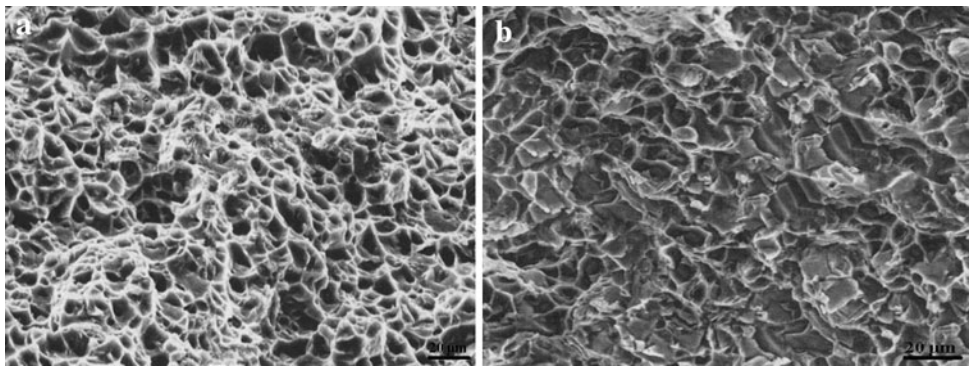

Fig. 8 Fracture surfaces obtained in a uniaxial tension test: (a) unreinforced A1 (A356), and (b) Al/15 vol.% B4C

deep and circular-shaped confirming the high ductility observed in the tensile studies. In the case of composite samples, fracture surfaces revealed the brittle mode of fracture, with clear evidence of particle cracking, interface debonding, and deformation constraint in the matrix.

References

1. S. Suresh, A. Mortensen, and A. Needleman, *Fundamentals of Metal Matrix Composites*, Butterworth-Heinemann, Stoneham, MA, 1993
2. R.L. Deuis, C. Subramanian, and J.M. Yelllup, Dry Sliding Wear of Aluminium Composites—A Review, *Compos. Sci. Technol.*, 1997, **57**, p 415–435
3. M. Rittner, *Metal Matrix Composites in the 21st Century: Markets and Opportunities*, BCC, Inc., Norwalk, CT, 2000
4. B. Venkataraman and G. Sundararajan, Correlation Between the Characteristics of the Mechanically Mixed Layer and Wear Behaviour of Aluminium, Al-7075 Alloy and Al-MMCs, *Wear*, 2000, **245**(1–2), p 22–38
5. Y. Iwai, T. Honda, T. Miyajima, Y. Iwasaki, M.K. Surappa, and J.F. Xu, Dry Sliding Wear Behavior of Al_2O_3 Fiber Reinforced Aluminum Composites, *Compos. Sci. Technol.*, 2000, **60**, p 1781–1789
6. M. Vedani, F. D'Errico, and E. Garibaldi, Mechanical and Fracture Behaviour of Aluminium-Based Discontinuously Reinforced Composites at Hot Working Temperatures, *Compos. Sci. Technol.*, 2006, **66**, p 343–349
7. R. Couturior, D. Ducret, P. Merle, J.P. Disser, and P. Joubert, Elaboration and Characterization of a Metal Matrix Composite: Al/AlN, *J. Eur. Ceram. Soc.*, 1997, **17**, p 1861–1866
8. S.C. Lim, M. Gupta, L. Ren, and J.K.M. Kwok, The Tribological Properties of Al-Cu/SiCp Metal-Matrix Composites Fabricated Using the Rheocasting Technique, *J. Mater. Process. Technol.*, 1999, **89 and 90**, p 591–596
9. M. Kouzeli and A. Mortensen, Size Dependent Strengthening in Particle Reinforced Aluminium, *Acta Mater.*, 2002, **50**, p 39–51
10. F. Thevenot, A Review on Boron Carbide, *J. Eur. Ceram. Soc.*, 1990, **6**, p 205–209
11. J.C. Viala and J. Bouix, Chemical Reactivity of Aluminium With Boron Carbide, *J. Mater. Sci.*, 1997, **32**, p 4559–4563
12. S.M.L. Nai and M. Gupta, Influence of Stirring Speed on the Synthesis of Al/SiC Based Functionally Gradient Materials, *Compos. Struct.*, 2002, **57**, p 227–233
13. J. Hashim, L. Looney, and M.S.J. Hashmi, Metal Matrix Composites: Production by the Stir Casting Method, *J. Mater. Process. Technol.*, 1999, **92/93**, p 1–7
14. A. Evans, C.S. Marchi, and A. Mortensen, *Metal Matrix Composites in Industry: An Introduction and a Survey*, Kluwer Academic Publishers, Dordrecht, Netherlands, 2003
15. A.J. Pyzik and I.A. Aksay, Processing and Microstructural Characterization of B4C-AI Cermets, US Patent No 4702770, 1987
16. N.A.El. Mahallawy, M.A. Taha, and M. Lofti Zamzam, On the Microstructure and Mechanical Properties of Squeeze-Cast Al-7 wt% Si Alloy, *J. Mater. Process. Technol.*, 1994, **40**, p 73–85
17. M. Kok, "Preparation and Some Properties of SiC Particle Reinforced Al Matrix", Ph.D. Thesis, The Institute of Science and Technology of Elazig University, Turkey, 1999
18. W. Zhou and Z.M. Xu, Casting of SiC Reinforced Metal Matrix Composites, *J. Mater. Process. Technol.*, 1997, **63**, p 358–363
19. S. Ray, Porosity in Foundry Composites Prepared by Vortex Method, *Proceedings of the Survey on Fabrication Methods of Cast Reinforced Metal Composites*, ASM/TMS, 1988, p 77–80
20. D.J. Lloyd and B. Chamberian, Properties of Shape Cast Al-SiCp Metal Matrix Composites, *Proceedings of the International Symposium on Advances in Cast Reinforced Metal Composites*, ASM, IL, 1988, p 263–269
21. F.M. Hosking, F. Folgar Portillo, R. Wunderlin, and R. Mehrabian, Composites of Aluminium Alloys: Fabrication and Wear Behaviour, *J. Mater. Sci.*, 1982, **17**, p 477–498
22. M. Roy, B. Venkataraman, V.V. Bhanuprasad, Y.R. Mahajan, and G. Sundararajan, The Effects of Particulate Reinforcement on the Sliding Wear Behavior of Aluminum Matrix Composites, *Metall. Trans. A*, 1992, **23**, p 2833–2846
23. S. Chung and B.H. Hwang, A Microstructural Study of the Wear Behaviour of SiCp/Al Composites, *Tribol. Int.*, 1994, **27**(5), p 307–314
24. S. Skolianos and T.Z. Kattamis, Tribological Properties of SiC-Reinforced Al-4.5% Cu-1.5% Mg Alloy Composites, *Mater. Sci. Eng. A*, 1993, **163**, p 107–113
25. P.N. Bindumadhavan, H.K. Wah, and O. Prabhakar, Dual Particle Size (DSP) Composites: Effect on Wear and Mechanical Properties of Particulate Metal Matrix Composites, *Wear*, 2001, **248**, p 112–120
26. Y.T. Zhao, S.L. Zhang, G. Chen, X.N. Cheng, and C.Q. Wang, In Situ (Al_2O_3 + Al_3Zr)np/Al Nanocomposites Synthesized by Magneto-Chemical Melt Reaction, *Compos. Sci. Technol.*, 2008, **68**, p 1463–1470
27. J.U. Ejiofor and R.G. Reddy, Characterization of Pressure-Assisted Sintered Al-Si Composites, *Mater. Sci. Eng. A*, 1999, **259**, p 314–323
28. Y.-C. Kang and S.L.-I. Chan, Tensile Properties of Nanometric Al_2O_3 Particulate-Reinforced Aluminum Matrix Composites, *Mater. Chem. Phys.*, 2004, **85**(2–3), p 438–443
29. S. Long, O. Beffort, C. Cayron, and C. Bonjour, Microstructure and Mechanical Properties of a High Volume Fraction SiC Particle Reinforced $AlCu_4MgAg$ Squeeze Casting, *Mater. Sci. Eng. A*, 1999, **269**, p 175–185
30. T. Christman, A. Needleman, and S. Suresh, Experimental and Numerical Study of Deformation in Metal-Ceramic Composites, *Acta Metall.*, 1989, **37**, p 3029–3050
31. Z. Wang and T.-K. Chen, Stress Distribution in Particle Reinforced Metal Matrix Composites, *Metall. Trans.*, 1993, **24A**, p 197–202
32. K.R. Suresh, H.B. Niranjan, P. Martin Jebaraj, and M.P. Chowdiah, Tensile and Wear Properties of Aluminum Composites, *14th International Conference on Wear of Materials*, August–September 2003, p 638
33. M.C. Watson and T.W. Clyne, The Tensioned Push-Out Test for Fibre-Matrix Interface Characterisation Under Mixed Mode Loading, *Mater. Sci. Eng. A*, 1993, **160**(1), p 1–5